DISCLAIMER

This report was prepared as an account of work sponsored by an agency of the United States Government. Neither the United States Government nor any agency thereof, nor any of their employees, makes any warranty, express or implied, or assumes any legal liability or responsibility for the accuracy, completeness, or usefulness of any information, apparatus, product, or process disclosed, or represents that its use would not infringe privately owned rights. Reference herein to any specific commercial product, process, or service by trade name, trademark, manufacturer, or otherwise does not necessarily constitute or imply its endorsement, recommendation, or favoring by the United States Government or any agency thereof. The views and opinions of authors expressed herein do not necessarily state or reflect those of the United States Government or any agency thereof. Reference herein to any social initiative (including but not limited to Diversity, Equity, and Inclusion (DEI); Community Benefits Plans (CBP); Justice 40; etc.) is made by the Author independent of any current requirement by the United States Government and does not constitute or imply endorsement, recommendation, or support by the United States Government or any agency thereof.

CASL-U-2014-0170-000

Power uprates and plant life extension

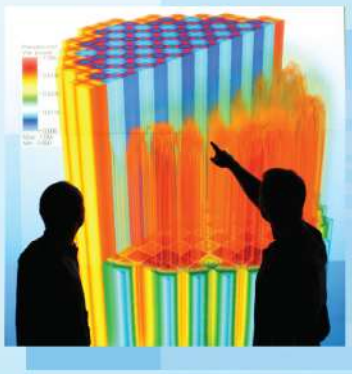

Engineering design and analysis

Science-enabling high performance computing

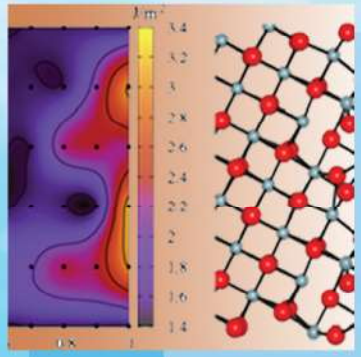

Fundamental science

Plant operational data

Consortium for Advanced Simulation of LWRs

L3:THM.P9.03

Integrated Lift- and Wall-Force Closures in Computational Fluid Dynamics (CMFD)

Thomas Daly and Art Ruggles
University of Tennessee-Knoxville

Sreekanth Pannala
Oak Ridge National Laboratory

August 29, 2014

CASL-U-2014-0170-000

U.S. DEPARTMENT OF ENERGY | Nuclear Energy

Integrated Lift- and Wall-Force Closures in CMFD

CASL Internal Report

Thomas Daly	Sreekanth Pannala	Art Ruggles
tdaly1@utk.edu	pannalas@ornl.gov	aruggles@utk.edu

August 29, 2014

CASL-U-2014-0170-000

1 Introduction and Background to Lift Forces in Bubbly Flows

In this report, we provide the necessary background to put this work in context and for a more detailed background, the reader is referred to CASL 2013 report ([1]).

Central constraints on the design of LWRs are thermal-structural limits, e.g., maximum fuel pin temperature and maximum allowable working pressure in a pressure vessel. In both of these cases, the knowledge of the spatially and temporally varying two-phase flow is required to make accurate predictions as the distribution of both the phases have an impact on heat extraction as well as neutron moderation.

Engineered two-phase flow systems have complex geometry and often high Reynolds numbers which increase the computational cost of an analysis, and generally make direct numerical simulations of the flow field impossible even on the fastest computers today. Consequently, a number of models which seek to reduce this computational cost have been created over the years. One of these called the two-fluid model has become the standard in three dimensional CFD (Computational Fluid Dynamics) codes and is also referred to as CMFD (Computational Multiphase Fluid Dynamics).

The two-fluid model splits each conserved quantity into two fields, one for each phase that is treated as interspersed continua. Splitting one field into two requires additional interfacial closure relationships. In the two-fluid model, the momentum flux between the phases is governed by a number of these closure relationships. Generally, the net force on the dispersed phase is decomposed into inertial, added mass, buoyancy, drag, lift, and wall forces. In addition, there is a time-dependent Basset force, as well as turbulent dispersion effects. The general form of force on a bubble can be written as [2]

$$\rho_b(\frac{4}{3}\pi a^3)\frac{du_b}{dt} = F_I + F_A + F_L + F_D + F_B \tag{1.1}$$

where F_I is the inertial force, F_A is the added mass term, F_L is the lift force, F_D is the drag force, and F_B is the buoyancy force or in its full form

$$\begin{aligned}\frac{du_b}{dt} =& \frac{1+C_M}{\gamma+C_M}\left(\frac{\partial v}{\partial t} + (v\cdot\nabla)v\right) + \frac{C_L}{\gamma+C_M}(v-u_b)\times\omega \\ &+ \frac{1}{\gamma+C_M}\frac{3C_D}{8a}|v-u_b|(v-u_b) + \frac{\gamma-1}{\gamma+C_M}g\end{aligned} \tag{1.2}$$

Here, u_b is the bubble velocity, v is the fluid velocity, C_M is the added mass coefficient, C_L is the lift coefficient, C_D is the drag coefficient, γ is the ratio of densities (ρ_b/ρ), g denotes gravity, and ω stands for vorticity. In general, the coefficients are not constant, although their functional dependence has not been explicitly stated. A few effects have

been ignored, including those due to time history, density gradients, and temperature gradients. Equation 1.2 is not based on a unified derivation of all these forces; rather, it is a composite of the various forces that have been found to act on the bubbles. In the current study, we will still use this superposition principle as an overall recast of the closure relations is not a trivial task.

One of the lesser understood momentum closures is that due to the transverse forces. These transverse forces are very critical for LWR applications as transverse motion of bubbles in the narrow and long flow channels between the fuel rods impacts heat transfer and neutron moderation. A lift force found to act on dispersed particles in tube-flow was first quantitatively described by Segré and Silberberg [3]. In their 1962 paper, they find that a solid sphere in Poiseuille flow experiences radial forces, and that there is a stable equilibrium radial position at approximately $0.6r/R$ under certain flow conditions. The radial equilibrium position for particles in this experiment shows that there are competing forces in the transverse direction which are of similar magnitude. Their quantitative findings have been superseded by newer, more finely grained experimental data; however, they gave impetus to the following decades of theoretical and experimental work.

Transverse forces are perpendicular to the relative velocity of the bubble with respect to the fluid and are commonly decomposed into lift and wall force contributions in the CMFD community. The lift force term is motivated by the physics, while the wall force term is added as a correction in order to ensure that there is no gas (bubble) accumulation very close to the wall. In practice this creates stability issues for a CMFD code as both effects are of similar magnitude as one approaches the wall, yet have very different dependencies on the local properties. This compartmental view of the total transverse force is an oversimplification which ignores the interplay between the two forces and the variation of the lift force as a function of distance from the wall. Figure 1.1 shows how the currently implemented lift and wall forces increase in magnitude significantly near the wall. These large values for the lift force are unphysical, and in general the coefficients of the wall force are tweaked in order to cancel the shear lift force at the wall. The shear lift force itself is overpredicted as one moves toward the wall, because the assumptions that were used in its derivation become invalid. More details about these assumptions are detailed in Section 1.1, where the theoretical work on the shear lift force, and its limits of applicability will be discussed. In Section 1.2, the literature related to computational simulations and experiments of bubble motion are detailed, in order to extend the closures to include more realistic scenarios. A brief review of the various options for lift and wall forces currently available in popular CMFD codes is provided in Section 1.3. In Section 1.4, we summarize the closure from last year and our new findings. Chapter 2 covers, data extraction, processing, and visualization; as well as introduces a new model of the lift force in the presence of walls. After the model's description, its behavior is tested and characterized using a turbulent pipe flow profile.

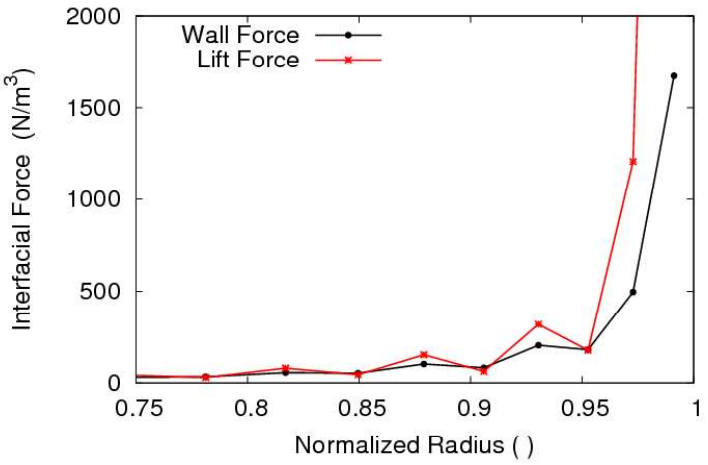

Figure 1.1: Lift/Wall forces near the wall of a bubbly pipe flow [4]

1.1 Theoretical Models of Shear Lift

Shear lift forces in general arise due to asymmetry in the flow field. Most theoretical work on shear lift force assumes a spherical body and then attempt to tease out a shear lift force that is valid under a certain range of flow conditions. Figure 1.2 shows a simple shear flow about a sphere; it is the base model used for most of the theoretical work on shear lift force. Far upstream, the liquid velocity is given by $v_\ell = U_\ell + Gy$, where v_r is the relative velocity at the center of the sphere, and G is the magnitude of the upstream vorticity. Due to complications in adding the effect of the wall, most of the theoretical work starts essentially with what is pictured in figure 1.2 where the effects of the wall are ignored.

Additionally, almost all of the theoretical predictions rely on perturbation methods, so understanding the magnitudes of dimensionless coefficients is important. The dimensionless parameters discussed in this section are shown in table 1.1. Reynolds numbers whose characteristic length is the diameter of the sphere, d, appear often, as well as dimensionless parameters describing the ratio of uniform to shear velocity. Note that most authors define their Reynolds numbers using diameter, but those based on radius also exist.

A number of papers which cover analytical work on particle lift force are shown in table 1.2. For high Re and small Sr an analytical lift force has been calculated for a sphere and a few bodies of revolution. The rest of the analytically-oriented papers are for low particle Reynolds number, and are based on Saffman's work, with the exception of the paper by Vassuer & Cox.

On the theoretical front there are essentially two streams of work on evaluating shear lift force: one looks at a low particle Reynolds number ($Re_p = \frac{v_r 2a}{\nu}$ or simply Re) flow of

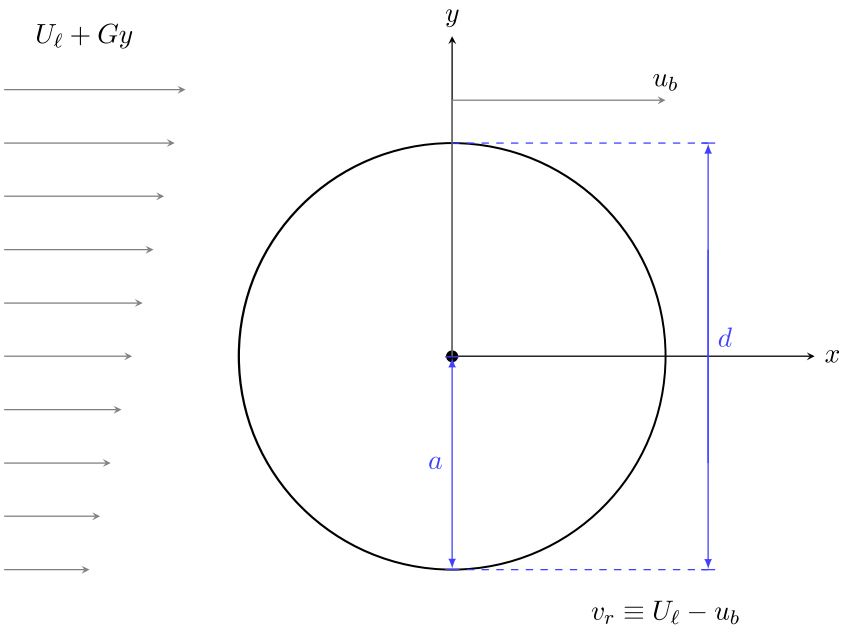

Figure 1.2: Shear Flow Around Sphere

Table 1.1: Dimensionless Parameters for Shear Lift

Name	Definition
Slip Re, Particle Re	$Re = \frac{dv_r}{\nu}$
Shear Re	$Re_G = \frac{d(Gd)}{\nu}$
Dimensionless Shear	$Sr = \frac{dG}{v_r}$
Ratio of Shear Re to Slip Re	$\epsilon = \frac{\sqrt{Re_G}}{Re}$
	Note that $Sr = \frac{\epsilon^2}{2} Re$

Table 1.2: Theory-based Lift Force Literature

Name	Re	Sr	Wall	Shape/Alignment
High Re and small Sr				
Auton [5]	High	Low	No	Sphere
Naciri [6]	High	Low	No	Bodies of revolution
Low Re				
Saffman [7]	Low	High	No	Sphere
McLaughlin [8]	Low	Low-High	No	Sphere
McLaughlin [9]	Low	Low-High	Yes	Sphere
Cherukat & McLaughlin [10]	Low		Yes	Sphere
Asmolov [11]	Low	Low-High	Yes	Sphere
Vasseur & Cox [12]	Low	Zero	Yes	Sphere

a simple shear around a sphere, while the other considers the inviscid limit of weak simple shear around a sphere. Below we elaborate the work on these two different streams.

1.1.1 Lift Forces at Low Reynolds Number

1.1.1.1 Shear Lift Force

The low Reynolds number regime was initially investigated by Saffman, who found that in the viscous limit, a simple shear flow about a sphere yields a lift force given by [7]

$$F_L = 81 \cdot 2\mu v_r a^2 G^{1/2}/\nu^{1/2} \tag{1.3}$$

where G is the magnitude of the shear and v_r is the relative velocity of the sphere. Although Saffman was able to come up with an analytical solution to the Oseen-like problem in a free stream, the effect of a wall remained unconsidered. Most of the additional theoretical work done since Saffman's paper has been for small Re_p. McLaughlin [9] has expanded on Saffman's work by including the effect of the wall, upstream vorticity curvature, while Asmolov [11] has included the effects of higher (but still laminar) channel Reynolds numbers.

Shear lift forces in general depend on where the relative velocity and shear are measured; usually the values are taken to be far upstream along a streamline that stagnates at the front of the body. In other words the relative velocity and shear rate are given by the far-field condition far upstream of the particle. A dimensionless shear Reynolds number used by Saffman, McLaughlin, and Asmolov is defined as $Re_G = \frac{4Ga^2}{\nu}$. Here G is the magnitude of the upstream vorticity, a is a characteristic length of the particle, and ν is the kinematic viscosity of the continuous phase. Saffman's work has a number of restrictive assumptions, including $Re_p \ll 1$ and $Re_G \ll 1$, but also $Re_p \ll Re_G^{1/2}$. His work assumes a large shear rate relative to the slip velocity.

McLaughlin [9] and Asmolov [11] built on Saffman's work by calculating the lift force on a particle in a linear shear flow in the presence of the wall. In McLaughlin's paper

from 1991 [8], he decomposes the migration velocity of the spherical particle into two contributions, one coming from unbounded shear flow and the other one due to wall effects, $v_m^u + v_m^w$, and the unbounded migration velocity comes from Saffman's lift force. The wall migration velocity is calculated for large l_* as $v_m^w = -0.2855aU(A/\nu)^{1/2}l_*^{5/3}$, where l_* is a dimensionless distance from the wall (based on the Saffman length $((\nu/A)^{1/2})$. They also relaxed the high shear assumption that Saffman's work assumes, and in the process adding a term, $J(\epsilon)$, to Saffman's lift force equation 1.3 in order to account for changes in the relative magnitudes of slip and shear Reynolds numbers. Two asymptotic expansions for $J(\epsilon)$ exist, but in general this term has to be evaluated numerically.

1.1.1.2 Wall Force - no shear

One low Re study that looks at the effect of the wall in isolation is by Vasseur & Cox [12]. In their paper, they consider the lateral migration of a spherical particle in a quiescent Newtonian fluid near a vertical wall. They find that the particle always migrates away from the wall; i.e., there is a transverse force pointing away from the wall. It is interesting to note that under similar conditions a sphere settling in a second order fluid (an approximation of viscoelastic effects) will experience a force pulling it towards the wall [13].

1.1.2 Lift Forces at High Reynolds Number

1.1.2.1 Shear Lift Force

For a clean bubble whose density is much less than that of the surrounding liquid, low Re approximations are not as applicable. Under high Re and low shear conditions, a lift force is generated by the deformation of oncoming vorticity around a body. It will be shown later that in this case the velocity can be written as an asymptotic series in dimensionless shear (Sr), and that the lift force arises from how the primary flow deforms the upstream vorticity. Figure 1.3 shows how the inviscid lift force arises through deformation of upstream vorticity. Note that under the inviscid assumptions Lighthill & Auton use no vorticity is generated at the surface of the body.

A number of researchers' work, primarily by Darwin [15] and Lighthill [16], over the course of 30 years culminated with Auton calculating the lift force on a sphere due to weak shear flow in an inviscid fluid [5] [17]. His analysis shows that the lift force in the inviscid limit about a sphere in a free stream has the form

$$F_L = \rho V_b C_L (v_\ell - u_b) \times (\nabla \times v_\ell) \tag{1.4}$$

and that the lift coefficient for a sphere is $C_L = \frac{1}{2}$, which happens to be equal to the added mass coefficient for a sphere. Here, V_b is the volume of the sphere and $v_\ell = U_\ell + Gy$ is the undisturbed liquid velocity far upstream of the sphere. The form of the lift force models by Auton and Saffman are similar, except that Auton's expression does not depend explicitly on viscosity and is proportional to G, while Saffman's expression for the lift force is proportional to $\sqrt{G}$. This raises the question about under what conditions

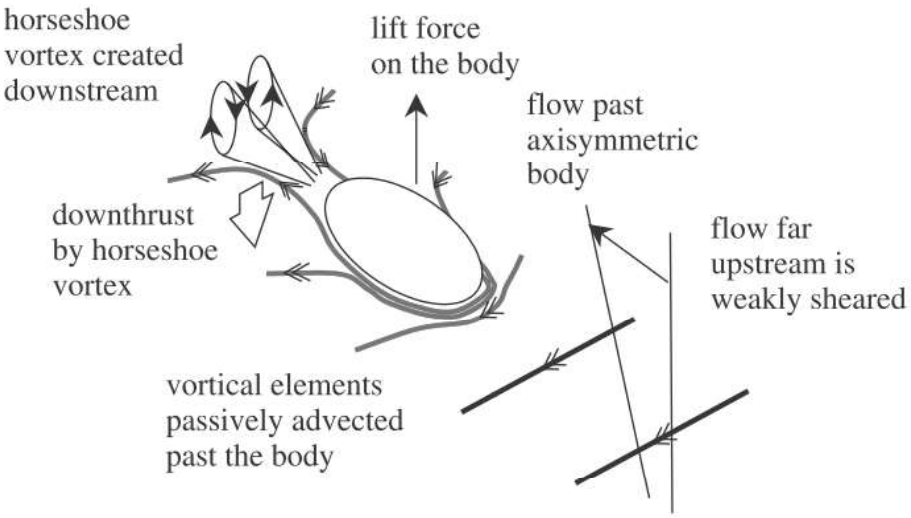

Figure 1.3: Vortex deformation by flow around body [14]

each of these correlations are applicable. This can be answered by analyzing the various assumptions in their derivation and also by comparing to the various experimental data at conditions where the underlying assumptions used in these derivations are not valid.

In comparison to the theoretical work done which builds on Saffman's model, there has been little theory-based studies or extensions for the inviscid shear lift force. Naciri [6] extended Auton's work by calculating the lift coefficient of several bodies of revolution. Interestingly enough, he finds that for the bodies considered C_L is found to be equal to the added mass coefficient (for a flow aligned with the axis of revolution of the body). We have recently derived that this result holds true even for arbitrary shaped particles and will document this result separately. Since there is little to no theory about how the inviscid shear lift force behaves under high shear, near the wall, or for arbitrary body shapes, many of these questions have been answered (at least in part) by a number of experimental and computational studies that are described in the next section.

1.2 Experimental & Computational Lift Force Literature

Most of the work presented here can be classified in two groups: the first one looks at particle or bubble distribution in a pipe or channel, and may sometimes include coarse trajectory information. This information is most useful for the validation of lift closure models in two-fluid CMFD codes. However, if the data shows that there are radial equilibrium points it can also be used as a guide to the relative magnitudes of the wall and shear lift forces, since at these positions the effects of the wall and shear lift forces should sum to zero. The other group focuses on calculating the lift force on a single particle given a number of flow parameters. Section 1.2.1 will focus on the former.

Most authors choose to represent their dimensionless lift force, C_L, as the lift coefficient that appears in Auton's model (Eqn 1.4). Away from the wall the lift force will vary from Auton's model as a function of Re and Sr, as in the derivation he assumes high Re and weak shear. This hints that the C_L coefficient based on Auton's work will require the largest correction in areas of low Re or high Sr.

Legendre & Magnaudet [18] use numerical simulations to calculate the shear lift force on a sphere over a wide range of Re and a few values of Sr. For $Re > 5$ and low to moderate shear rates ($Sr < 0.2$) they present a correlation describing the lift coefficient as purely a function of Re.

$$C_L = \frac{1 + 16Re^{-1}}{2(1 + 29Re^{-1})} \tag{1.5}$$

In the limit as $Re \to \infty$, their correlation recovers Auton's result of $C_L = 1/2$. In the last few years Rastello, et al. [19] [20] have conducted experiments and calculated bubble lift force in a solid body rotating flow. Their results line up well with those of Legendre & Magnaudet, although they find that for smaller Re their data is not fit well by Legendre & Magnaudet's correlation. Rastello, et al., give a correlation for C_L on a roughly spherical bubble as

$$C_L = 0.5 + 4\left(1 - \frac{6}{5Re^{1/6}}\right) exp(-Re^{1/6}) \tag{1.6}$$

1.2.1 Effects of Shear Rate, and Deformation

A study by Tomiyama, et al. [21] found a significantly smaller value (~0.3) for a lift coefficient, even for roughly spherical bubbles. Their lower value for C_L is most likely attributable to proximity to the wall and higher shear rates; however, it is not accurate far away from a wall or for lower shear values – the conditions under which the model was derived. From this perspective, the study shows how an increased shear and proximity to a wall will decrease the lift coefficient. Auton's model (with a constant coefficient) will overpredict the shear lift force as Sr becomes larger and the distance to the wall becomes important. For large values of Sr there is no theoretical work in the inviscid region; however, for small Re and high Sr Saffman finds that the shear lift force becomes proportional to $\omega^{1/2}$, while Auton's low Sr model is proportional to ω.

Large deformation has been found in some cases to even reverse the sign of the lift force [19], although under other conditions it increases the lift relative to a sphere. It is still not understood particularly well. Deformation changes the lift force in a few different ways, most notably the fact that deformation leads to asymmetrical shape of the body and the orientation to the flow becomes important. To understand how deformation affects the lift force, both shape and orientation must be taken into consideration. One application-driven concern of this phenomena is how a deformation based closure can be implemented in a two-fluid CMFD code where an ideal closure will only depend on local properties. Since the two-fluid model does not track phase boundaries, even if one can calculate the deformation of bubbles accurately, the orientation of the bubble still needs to be described in order to create a physical closure. Most likely there are one or more

preferred or stable orientations for a given body based on local properties like Re and Sr. If this is the case then the lift coefficient can be seen as a function of the deformation, χ, and these local properties. Rastello, et al., created a correlation to include the effects of deformation given by

$$C_L = C_L^{spherical} + 0.8(\chi - 1) - 1.3\frac{(\chi - 1)^{3/2}}{1 + 0.004Re^{3/2}} \tag{1.7}$$

where χ is the bubble's aspect ratio ($1 \leq \chi \leq 3$). In these experiments with lower shear, the lift force is actually found to increase with deformation.

1.2.2 Effects of the wall

If one looks at the effect of the wall in the absence of a primary flow, a few phenomena give rise to a lift force away from the wall. Zeng, et al., created a number of numerical simulations of a sphere moving in an otherwise quiescent fluid [22]. Figure 1.4 contains plots of streamlines at high and low Re at two distances from the wall. In addition, a recent CASL report [23] by Fang, et al., provides additional data on variation of the lift force coefficient as a function of distance of wall in uniform shear field at Re approaching PWR conditions. Parts (a) through (c) show a blockage type effect, where the flow is

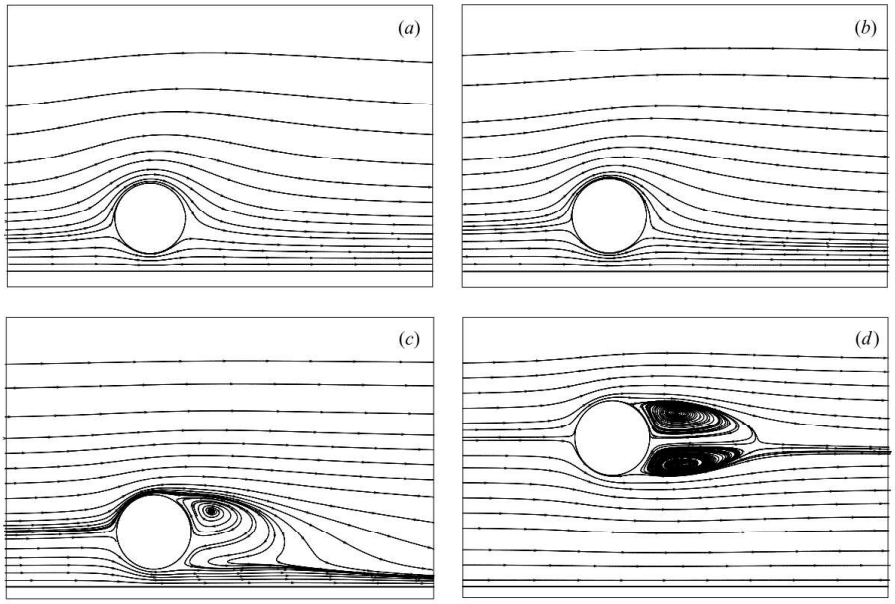

FIGURE 3. Streamlines plotted along the symmetry plane $y = 0$: (*a*) $Re = 2$, $L = 0.75$; (*b*) $Re = 10$, $L = 0.75$; (*c*) $Re = 200$, $L = 0.75$; (*d*) $Re = 200$, $L = 2$.

Figure 1.4: Streamlines around sphere near wall [22]

accelerated close to the wall. In part (d) at $L = 2$ and high Re the blockage effect is not as prevalent, but it is clear that the wake is asymmetric.

Now in the more interesting case where the continuous fluid is moving, the added complication of shear arises. Since G becomes very large at the wall, the assumption in Auton's model that $Sr \ll 1$ becomes invalid in many cases. Additionally, in pressure driven channel flow the curvature of upstream shear relative to the radius of the bubble, a, can not always be approximated as linear. Consequently, if Auton's model in its base form is to be used near the wall the lift coefficient should have a dependency on Sr, the dimensionless shear, or a similar measure.

1.3 Current Closure Implementation in CMFD Codes

Many widely used two-fluid CMFD codes, such as Ansys' CFX & Fluent, Star-CCM+, and NPHASE-CMFD, implement Auton's shear lift and Antal's wall force model as the two base lift forces. All allow the user to tweak the coefficients in the models, although by default the coefficients are constants.

Some codes also include a few correlations for the model coefficients by default. For example, Fluent includes lift coefficient, C_L, models by Legendre [18], Tomiyama [21], Mei [24], and Moraga. Moraga and Mei's models for C_L both include dependency on the shear Reynolds number, while Tomiyama's model is the only one to include the effect of deformation. In addition, the Fluent code includes models that modify Antal's wall force closure, developed by Frank, Hosokawa, and Tomiyama.

Table 1.3 presents a few shear lift force correlations. The models created by Mei & Clausner, Legendre & Magnaudet, and Rastello et al., all approach $C_L = 1/2$ as $Re \to \infty$. However, their low Re behavior is somewhat different. Rastello's low Re data come from a number of experiments in a solid body rotation, while Legendre & Magnaudet's data is from DNS simulations of simple shear around a sphere, and Mei & Klausner's low Re behavior is linked to McLaughlin's [8] findings.

Table 1.3: Lift Force Correlations

Name	Lift Coefficient
Mei & Klausner [24]	$C_L^D = F_L/(\frac{1}{2}\pi a^2 \rho U_r^2)$ $C_L^D = \sqrt{Sr}\left(\left[\frac{1.72J(\sqrt{2Sr/Re})}{\sqrt{Re}}\right]^n + \left[\frac{4Sr^{1/2}}{3}\right]^n\right)^{1/n}$ Correlation combines low & high Re theory; $n = 2$ suggested
Legendre & Magnaudet [18]	$C_L = \sqrt{(C_L^{lowRe})^2 + (C_L^{highRe})^2}$ $C_L^{lowRe} = \frac{6}{\pi^2}(Re \cdot Sr)^{-1/2} J'(\epsilon)$, where $J'(\epsilon) = \frac{2.255}{(1+0.2\epsilon^{-2})^{3/2}}$ $C_L^{highRe} = \frac{1+16Re^{-1}}{2(1+29Re^{-1})}$
Tomiyama et al. [21]	$Eo_d = \frac{g(\rho_L - \rho_G)d_H^2}{\sigma}$ $C_L = min[0.288tanh(0.121Re), f(Eo_d)]$ if $Eo_d < 4$ $C_L = f(Eo_d)$ if $4 \leq Eo_d \leq 10.7$ where $f(Eo_d) = 0.00105Eo_d^3 - 0.0159Eo_d^2 - 0.0204Eo_d + 0.474$ and d_H is the maximum horizonal diameter
Rastello et al. [19]	$C_L = 0.5 + 4(1 - \frac{6}{5Re^{1/6}})exp(-Re^{1/6})$ for sphere, low-high Re, low-med Sr $C_L^{deform} = C_L + 0.8(\chi - 1) - 1.3\frac{(\chi-1)^{3/2}}{1+0.004Re^{3/2}}$ for deformable bubbles where χ is the aspect ratio of the bubble

1.4 Closure developed during last year

In the previous year, we have developed the following closure assuming that the lift force goes to zero as the bubble touches the wall as there was not sufficient data (except for couple of points from [23]).

$$J(Sr, Re) = \frac{2.255}{(1 + 0.2Re/Sr)^{3/2}} \tag{1.8}$$

$$C_L^{low} = \frac{6J(Sr, Re)}{\pi^2 \sqrt{ReSr}} \tag{1.9}$$

$$C_L^{high} = \frac{1}{2}\left(\frac{1 + 310/Re - 242/Re^2}{1 + 176/Re + 566/Re^2}\right) \tag{1.10}$$

$$C_L^{nowall} = \sqrt{C_L^{low^2} + C_L^{high^2}} \tag{1.11}$$

$$C_L = C_L^{nowall} \log_2\left(\frac{E}{1 - E} + 2\right)^{-2.3} \tag{1.12}$$

During the beginning of this year, we have implemented this lift force in both Star-CCM+ as well as OpenFOAM. We still noticed the oscillations similar to that found by Fullmer (Figure 1.1). This forced us to re-evaluate the assumption of zero lift force at one bubble radius from the wall. In order to do that we performed several OpenFOAM simulations of a fixed sphere with varying distance from the wall and integrated the pressure on the sphere to extract the lift force. This data along with some new data from ITM-DNS from Bolotnov's group guided us to development of a new integrated lift-wall force closure described in the next section.

2 New Lift Force Closure

In this chapter an integrated shear lift- and wall-force closure is developed and presented. The form of the closure is based on theoretical work by Auton, Saffman, and others, with empirical corrections from physical experiments and computational simulations of resolved flow over spherical bubbles. The integrated lift closure is developed in three parts:

1. a shear-lift force closure which does not include the effects of the wall,
2. a wall-force closure, and
3. their smooth combination through a switching function

After development, the closure is compared to other models from the literature. Practical testing of the model is done in the following Chapter, where the closure is implemented in the OpenFOAM solver *twoPhaseEulerFoam* and compared to results of bubbly flow experiments taken from the literature.

The data on which the closure rests are broadly taken from two areas: theory and single-bubble studies. Most of the theoretical work in deriving lift and wall forces uses perturbation theory heavily. The perturbation parameters are usually the particle Reynolds number, a dimensionless shear rate, or some dimensionless measure of distance from the wall. As a consequence, the results from this theoretical work are only valid for very small (or large) values of these parameters. This leaves a large hole in the middle of the parametric space, which needs to be filled in with data from experiments or computational studies of the forces on a single bubble. Single bubble studies quantitatively describe the forces on a bubble or particle under a range of different flow conditions, e.g., by varying Reynolds number, dimensionless shear, distance to wall, or bubble deformation. These studies are often physical experiments, where the flow properties and movement of bubbles are tracked optically using high speed cameras. Other single-bubble studies are computational in nature. Here the flow around a spherical bubble is calculated and the resultant net force on the bubble is found.

2.1 Experimental Data Sources and Processing

Single-bubble experiments and computational simulations have been taken from the following papers.

- Numerical and experimental investigation of the lift force on single bubbles [25]

Table 2.1: Dimensionless parameters

Name and definition	Description
$Re = \frac{dv_r}{\nu}$	Particle reynolds number
$Sr = \frac{dG}{v_r}$	Dimensionless shear
$E = \frac{d}{2L}$	Dimensionless distance from wall
$C_L = \frac{F_L}{\rho\frac{\pi}{6}d^3 v_r G} = \frac{F_L}{\rho\frac{\pi}{6}\nu^2 Re^2 Sr}$	Auton lift coefficient
$C_{LD} = \frac{F_L}{\rho\frac{\pi}{8}d^2 v_r^2} = \frac{F_L}{\rho\frac{\pi}{8}\nu^2 Re^2}$	Drag law type lift coefficient

- ITM/DNS database of drag, lift and wall effects, including the effects of void fractions [23]
- Drag and lift forces on a spherical particle moving on a wall in a shear flow at finite Re [26]
- The lift force on a spherical bubble in a viscous linear shear flow [18]
- Drag and lift forces on clean spherical and ellipsoidal bubbles in a solid-body rotating flow [19]
- Drag and lift forces on bubbles in a rotating flow [27]

In addition, we have created our own single-bubble simulations using the OpenFOAM solver *simpleFoam*.

This data has been read in through various python scripts which keep track of the different dimensional and non-dimensional parameters used in each of the references. We have also collected a lot of data from other references not listed here but were not able to use it as they did not have all the necessary parameters to translate into a standard set of non-dimensional parameters. The dimensional parameters that are used in the work here are listed in table 2.1 and we have introduced a new parameter E that makes the distance from the wall non-dimensional. We have chosen this form as it would reach 1 as the bubble touches the wall and goes to 0 as the bubble is far away from the wall. For our purposes (with no deformation, boiling or other considerations), the four non-dimensional parameters that describe the lift force data are: $Re, Sr, E, and\, C_L$. The relevant dimensional parameters are described in figure 2.1. The python scripts read the data from the above cited papers and transform them to be described in this dimensionless group.

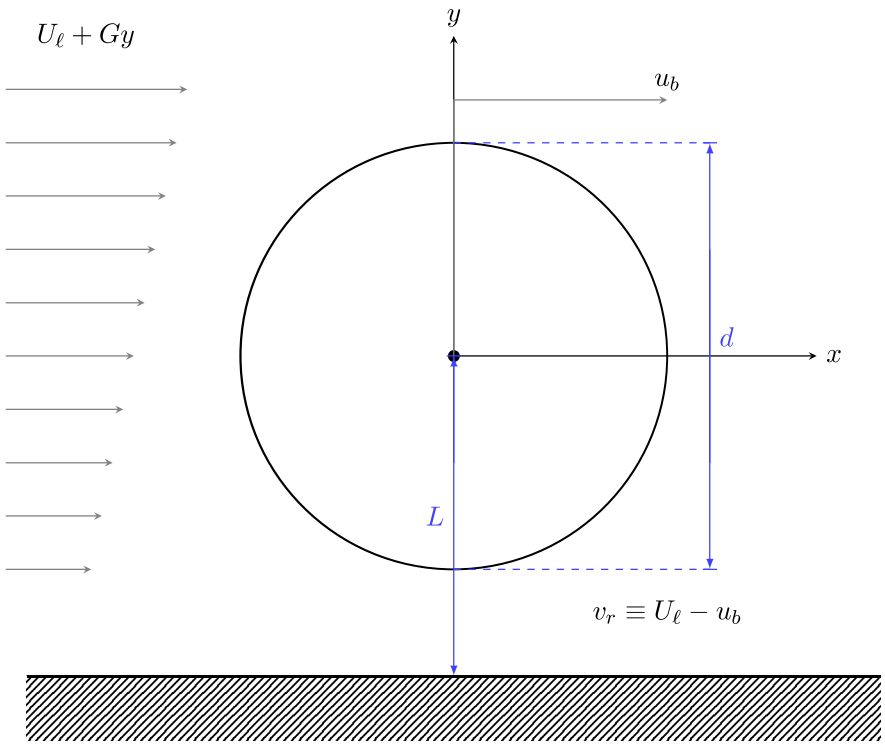

Figure 2.1: Sketch of the system along with the various dimensional parameters for relevance

2.2 Data Visualization

We present the data extracted above in few different ways to understand the behavior the lift force as a function of the these four different non-dimensional numbers.

In figure 2.2, we plot C_L as a function of independent non-dimensional variables $E, Sr, and\, Re$. The data in these plots does not follow any particular trend.

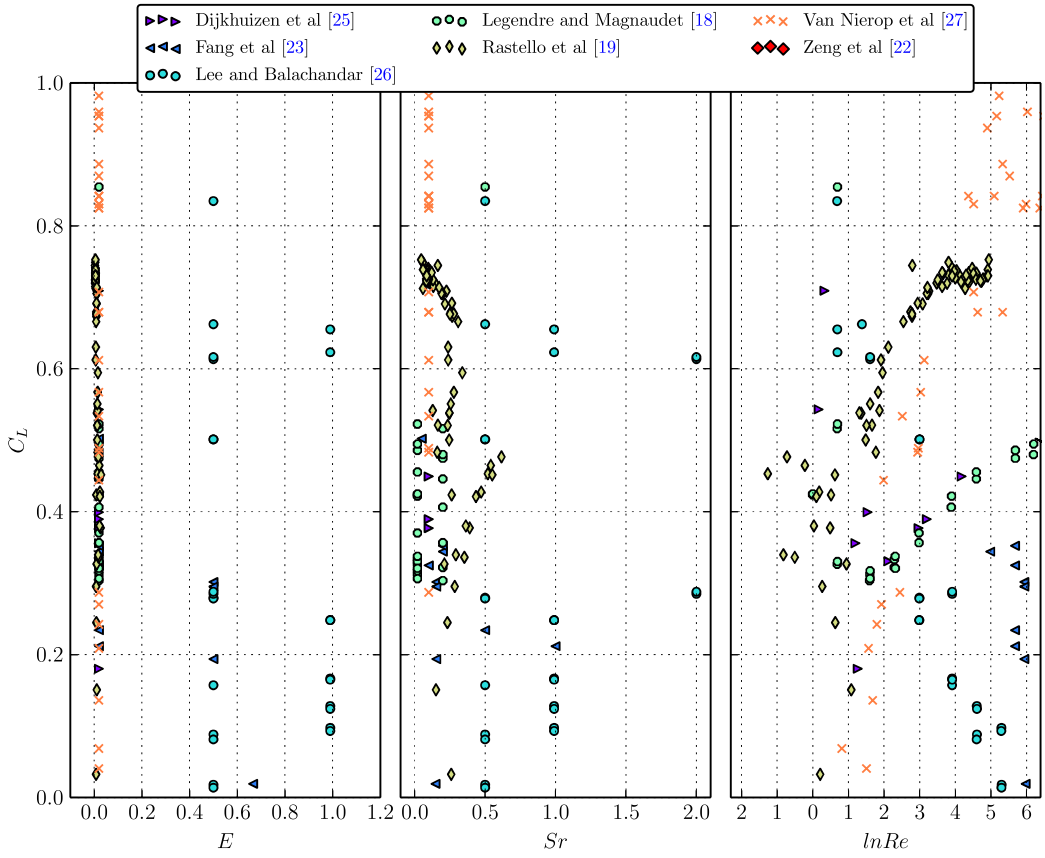

Figure 2.2: Plot of data points showing C_L over the independent variables

Now that we have the data, we can also look at scatter plots by projecting the data onto two variables. For e.g., $E\, and\, Sr$ are plotted in figure 2.3.

At a glance, the above data is very difficult to visualize and work with. We have normalized the data in various ways and also looked at correlation between C_L and various combinations of the variables. This gave us some insight into how to collapse this data and that procedure is described in the next section.

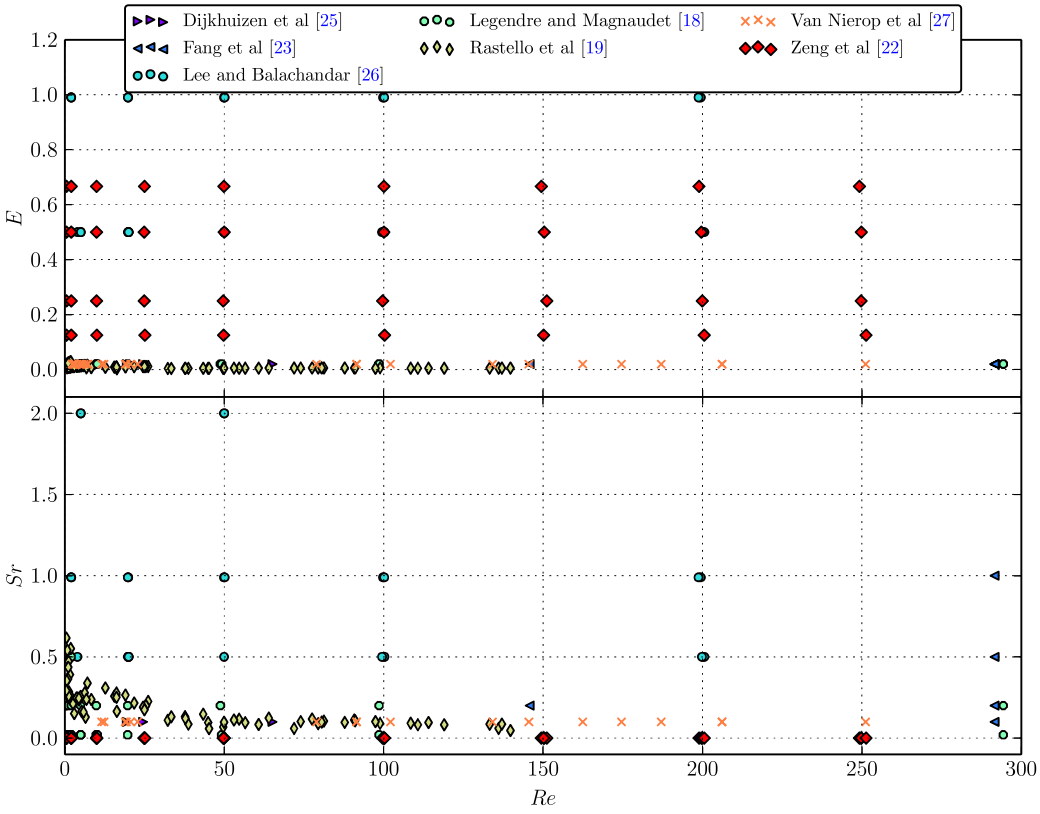

Figure 2.3: Plot of data points showing distribution of Sr and E

2.3 Constructing Correlations for Lift

As a starting point, we take the following closures that have good limiting behavior under certain constraints:

- Drag and lift forces on clean spherical and ellipsoidal bubbles in a solid-body rotating flow [19]
- The lift force on a spherical bubble in a viscous linear shear flow [18]
- Migration and deformation of bubbles rising in a wall-bounded shear flow at finite Reynolds number[28]
- Shear lift force on spherical bubbles[24]

These closures along with the experimental data are plotted in figures 2.4 and 2.5. We have divided this into two different Re regions as the variation in C_L is quite dramatic at low Re but asymptotically reaches 0.5 for large Re. In addition, we color the symbols with E so that one can visualize the scatter due to different E. As you can see existing closures do not capture the effect of all the different parameters and are good over certain range. For example, Rastello's model is good at moderate to large Re and away from the wall but very poor at very low Re.

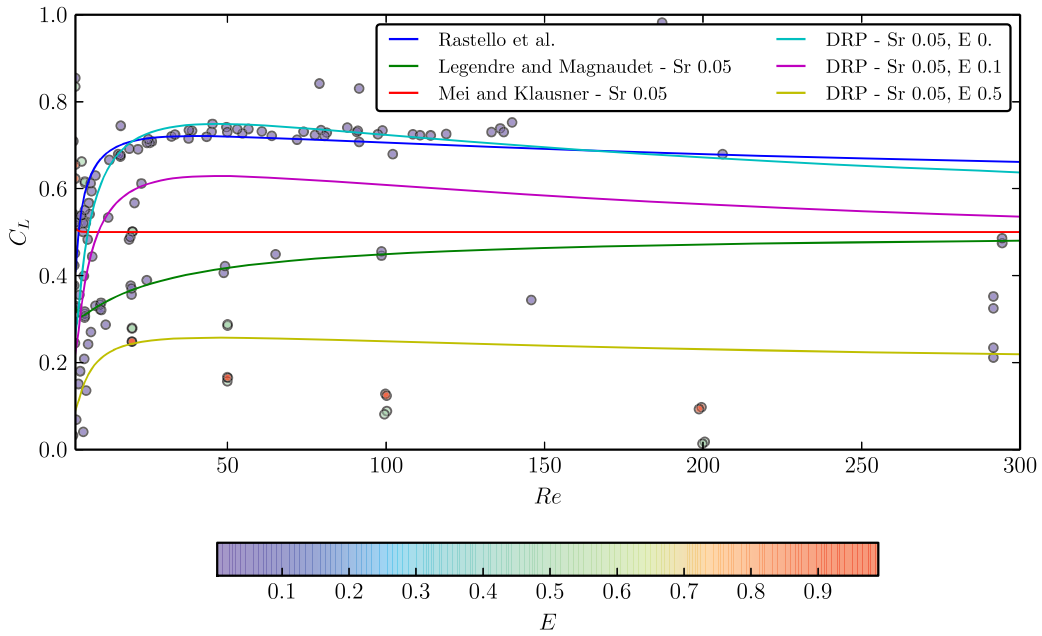

Figure 2.4: Lift coefficient over $Re > 10$ with models

With the above closures as the starting point, we wanted to capture all the corners of the 4-dimensional map asymptotically. Based on existing closures, we could capture the behavior of C_L versus Sr and Re. So we went ahead and introduced a form that captures the behavior of C_L versus E by looking at the correlation of different functional forms of E and picked several forms that give high correlation. Out of all the 8 different versions we have tried, below we present the correlation that matches the data very well in a least-square sense. The new DRP lift closure is also plotted in figures 2.4 and 2.5. The terms in the correlation that do not include the distance to the wall are based on Legendre & Magnaudet's model, with the addition of two additional parameters in the C_L^{high} term. The closure for C_L^{nowall}, which does not include any dependence on the wall, was described in more detail in the previous CASL report [1], and is found to match experimental and theoretical results closely.

$$J(Sr, Re) = \frac{2.255}{(1 + 0.2Re/Sr)^{3/2}} \tag{2.1}$$

$$C_L^{low} = \frac{6J(Sr, Re)}{\pi^2\sqrt{ReSr}} \tag{2.2}$$

$$C_L^{high} = \frac{1}{2}\left(\frac{1 + 310/Re - 242/Re^2}{1 + 176/Re + 566/Re^2}\right) \tag{2.3}$$

$$C_L^{nowall} = \sqrt{C_L^{low^2} + C_L^{high^2}} \tag{2.4}$$

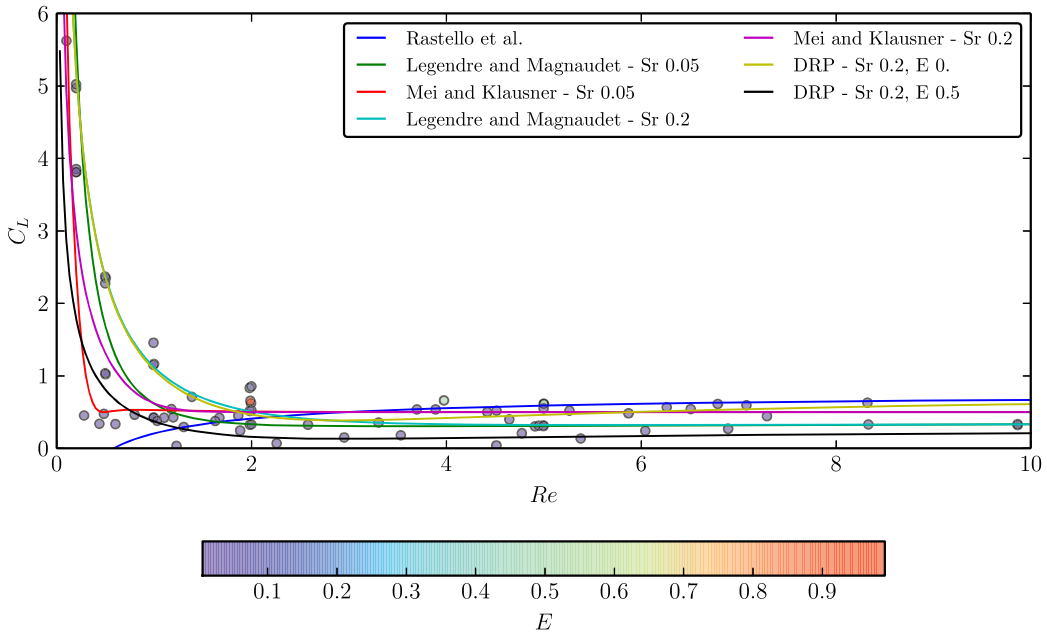

Figure 2.5: Lift coefficient over $Re < 10$ with models

2.4 Combining the shear-lift model with wall force

Now that a model for the shear induced lift force has been selected, the remaining tasks in creating a unified transverse force are to first create a wall model, and finally choose a smoothing function to switch between the shear- and wall-force contributions. Mathematically, this can be written as

$$C_{LD}^{Combi} = ((1-\alpha)C_L^{nowall}\frac{4}{3}\mathbf{Sr}) + (\alpha C_{LD}^{Wall}\mathbf{n}) \tag{2.5}$$

where $\mathbf{Sr}$ is the vector dimensionless shear rate, and $\mathbf{n}$ is the wall normal. The shear-lift term contains the factors $\frac{4}{3}\mathbf{Sr}$ which arise due to the conversion to the drag-law type coefficient C_{LD}. The function $\alpha = \alpha(Sr, E)$ has a range between zero and one, and allows for the smooth transition between shear lift and and wall effects.

The simplest model which achieved very low MSE was a parametric model of the form $C_{LD}^{Wall} = C_0$ and $\alpha(Sr, E) = E^{C_1}$, where C_i are constants. The calculated coefficients are shown in table 2.2. The wall coefficient is calculated to be approximately 1/2 or the added mass coefficient of a sphere. This result is also derived in Lamb's book on hydrodynamics [29]. However, the data used in this regression is sourced from cases with high particle Reynolds numbers ($Re > 100$), and Lamb's results are based on inviscid theory. So this static wall coefficient is really only accurate for moderate to high Reynolds number. A more complicated and comprehensive wall model could be sourced from Antal [30] or Frank [31].

Table 2.2: Model Coefficients

Name and definition	Description
$C_{LD}^{Wall} = C_0 = 0.50 \pm 0.01$	Wall coefficient
$C_1 = 4.9 \pm 0.1$	Coefficient found in $\alpha(E)$
$\alpha(E) = E^{4.9}$	Switching function

The form for the α function as E^{C_1} was chosen, because it performed similarly or better than more complicated models like $E^{C_2+C_3Sr}$. Using this form for α and plugging in the coefficients found in Table 2.2 the combined lift-wall coefficient can be written as

$$C_{LD}^{Combi} = ((1 - E^{4.9})C_L^{nowall}\frac{4}{3}\mathbf{Sr}) + (E^{4.9}\frac{1}{2}\mathbf{n}) \tag{2.6}$$

The output from the C_{LD}^{Combi} model is plotted against its training data in Figure 2.6; it displays uniformly acceptable error, although its performance is best when $E < 0.8$.

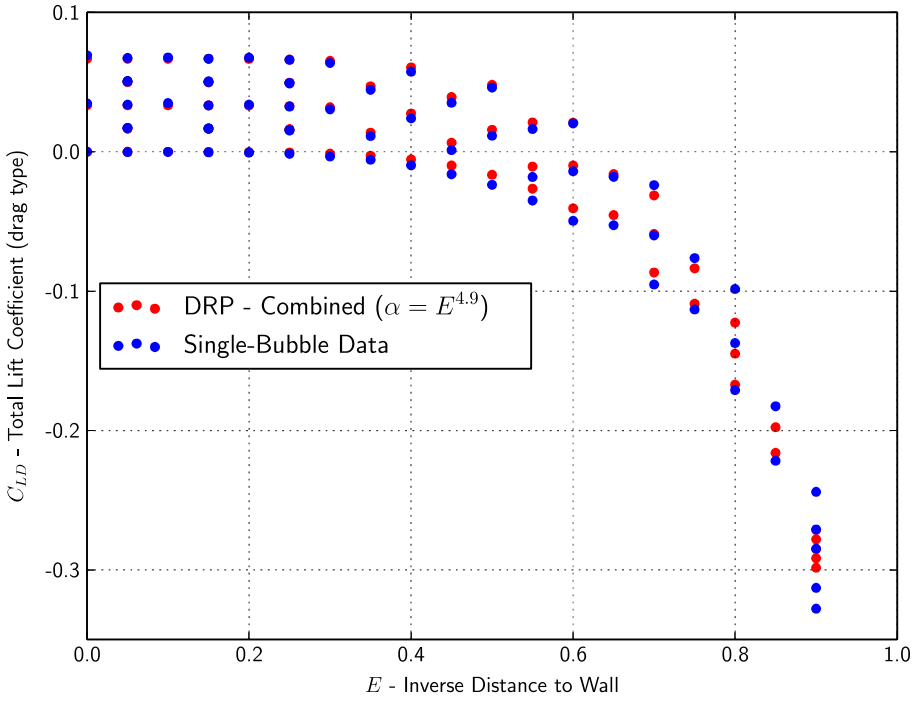

Figure 2.6: Total Lift for Single-Bubble Computational Studies and Proposed Model

The shear and wall lift forces are used in the code *twoPhaseEulerFoam* after being cast in their drag forms. This is necessary for numerical stability for regions where Sr approaches zero.

2.5 Applying the Lift Closure to Turbulent Pipe Flow

Now that we have a new closure for lift that captures the existing experimental and computational DNS data quite well, we want to test it out for a turbulent pipe flow. Before one can test it out in an actual CMFD model of two-phase turbulent flow, we have chosen the standard approximation of the $1/7^{th}$ formula for the velocity profile in a turbulent pipe flow to get the qualitative behavior of the current closure in comparison to a few existing closures.

Figure 2.7 shows the relative forces of five different lift-force closures with particle Reynolds number set to 100, a channel diameter of 5.715 cm, and a bubble diameter of 3 mm. From the center of the channel ($r/R = 0$) to $r/R = 0.5$ all yield a force within a few percent of each other. It is not until $r/R = 0.7$ (see Fig. 2.8) that the differences become noticeable, and until $r/R > 0.9$ when the wall correction changes the sign of the lift-wall combination models. Since the wall correction is a function of E, the absolute distance to the wall where the combined model becomes zero is dependent on bubble diameter; smaller bubbles will cross zero force nearer to the wall than larger bubbles.

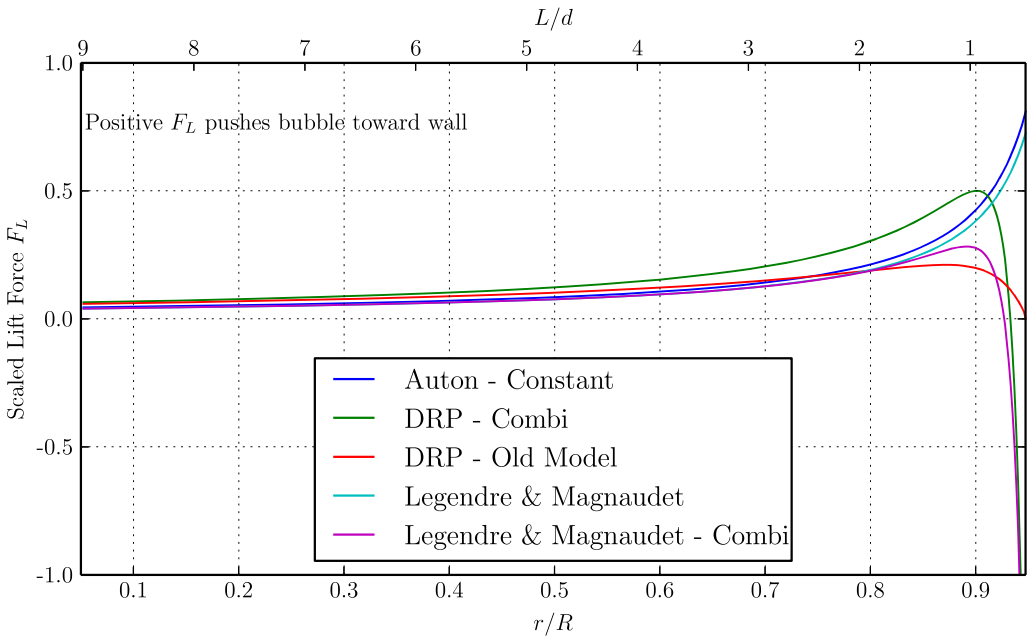

Figure 2.7: Lift force comparison between different closures in a turbulent pipe flow

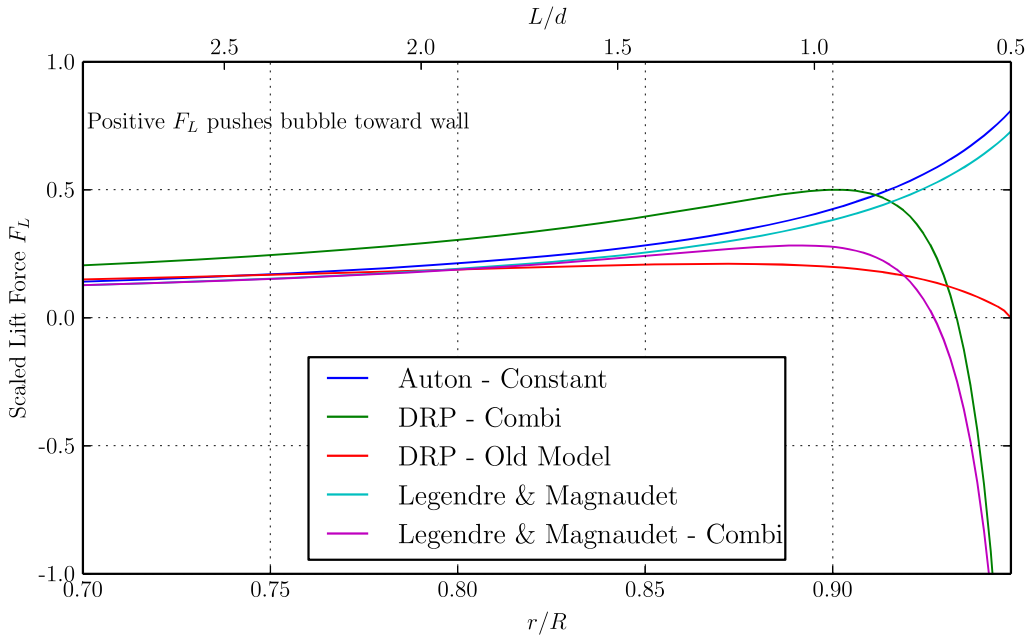

Figure 2.8: Lift force comparison between different closures in a turbulent pipe flow, near-wall region

2.6 Model Implementation in OpenFOAM

The CFD code OpenFOAM contains a transient solver of the two-fluid model equations called *twoPhaseEulerFoam*. The combined lift-wall force model given by Equation 2.6 has been implemented as optional interfacial forces in the solver. Using this code a number of cases have been run and analyzed using various lift and turbulence models. The boundary conditions are based on the bubbly flow experiments by Wang et al.[32]. As *twoPhaseEulerFoam* is a transient solver, all of the results have been averaged over a sufficiently long period of time.

Figure 2.9 shows the void fraction at a specific height above inlet for cases with different lift and turbulence models. With the exception of these models the cases are identical. The models used in each case are given in Table 2.3. Similar to the results found by plugging the models into a simple turbulent profile, the void fraction is found to be similar for all models near the center of the channel, while results diverge close to the wall.

A better view of void fraction in the near-wall region can be seen in Figure 2.6. The cases with no lift yield a flat profile across the channel, while the cases using Legendre & Magnaudet's shear lift cause bubbles to accumulate on the wall. Using the combined lift-wall model yields a void-fraction peak in same radial location as the corresponding experiment by Wang et al, although the heavy shear in the turbulent case causes the lift component to be larger, and as a consequence the peak is more sharply defined. This new formulation is found to more closely predict the physics found in actual bubbly flow experiments, while simultaneously removing instabilities due to the mismatch of lift and wall forces.

Table 2.3: Case List

Case Name	Lift Model	Wall Model	Turbulence Model
legendre_antal	Legendre	Antal	Laminar
dprCombi_turb	DPR - Combi.	None (built-in to lift)	$k-\epsilon$
nolift	None	None	None
dprCombi	DPR - Combi.	None (built-in to lift)	Laminar
nolift_turb	None	None	$k-\epsilon$
legendre	Legendre	None	None

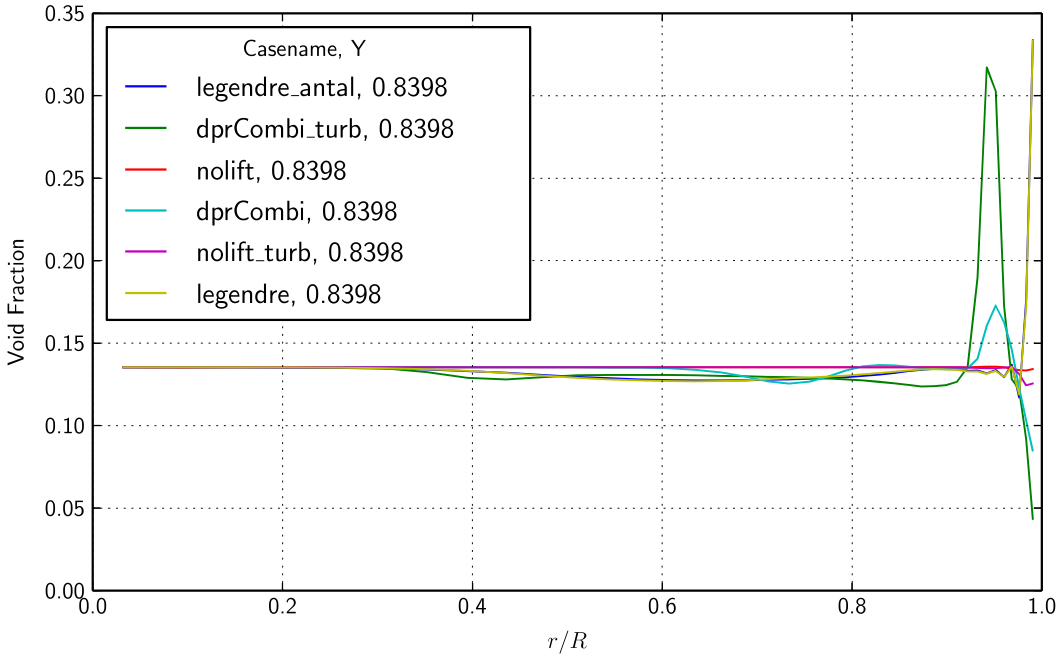

Figure 2.9: Various Lift Models - Void Fraction over Radial Distance in Concurrent Upflow

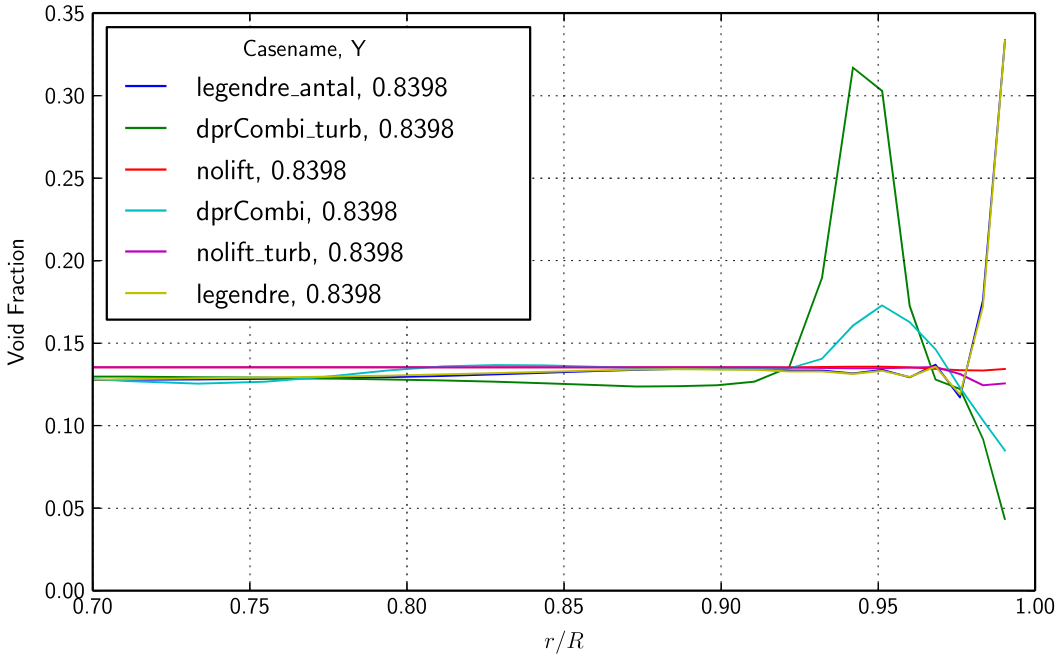

Figure 2.10: Various Lift Models - Void Fraction over Radial Distance in Concurrent Upflow, Near-Wall Region

2.7 Conclusions

The shear lift coefficient developed previously and given in this paper by C_L^{nowall}, has been extended and worked into a new model which includes wall effects. This new model C_{LD}^{Combi} smoothly switches between shear-lift and wall force components, in doing so it reduces instabilities produced by competing lift and wall forces.

The combined lift-wall model's implementation in OpenFOAM also underscores the importance of the drag and turbulence model on the overall results of void fraction distribution. This is because the shear lift force model depends essentially linearly on the dimensionless shear rate Sr and relative velocity v_r, while the wall model is proportional to the square of the relative velocity. In order to get accurate predictions these models must also be correct.

The proposed model shows good results for small, roughly spherical bubbles. However, for different shapes and orientations it needs to be modified. There are a few correlations by Tomiyama [21] and Rastello [19] that include some dependency on deformation of the bubble, but they're not sufficient for all flow conditions. There is also little theoretical work that evaluates the lift coefficients for different shapes and orientations.

2.8 Future Work

The correlation developed here is only the initial formulation and additional work is needed to put this on a strong theoretical footing and also include additional effects encountered in a PWR. Additional work in validating this model, and in testing other similar formulations against experiments is still necessary. These next steps include a closer look at drag and turbulence models, as these models strongly influence the resultant flow properties, particularly when lift models are included. Their dependence on void fraction and bubble swarming needs to be more closely understood.

Another development path for a combined lift- and wall-force closure is to start with a more fully developed wall force model, as the one proposed in this paper is based on high Re experiemnts. This model could then be combined with the shear lift force using a function similar to $\alpha(E)$ which switches between the shear and wall model. Bubble deformation has a strong effect on shear lift, and can even switch the sign of the force. As such deformation is another important avenue to explore in creating a integrated lift-wall closure which is robust and leads to physically accurate predictions.

Bibliography

[1] T. Daly, S. Pannala, and A. Ruggles. Lift forces in bubbly flows. Technical report, CASL, 2013.

[2] J. Magnaudet and I. Eames. The motion of high-reynolds-number bubbles in inhomogeneous flows. *Annual Review of Fluid Mechanics*, 32(1):659–708, 2000.

[3] G. Segre and A. Silberberg. Behaviour of macroscopic rigid spheres in poiseuille flow part 2. experimental results and interpretation. *Journal of Fluid Mechanics*, 14(01):136–157, 1962.

[4] W Fullmer, S Pannala, and I Bolotnov. Initial assessment of nphase-cmfd for application to adiabatic bubbly two-phase pipe flow. Technical report, CASL, 2011.

[5] TR Auton. The lift force on a spherical rotational flow. *J. Fluid Mech*, 183:199–218, 1987.

[6] Ahmed Naciri. *Contribution l'tude des forces exerces par un liquide sur une bulle de gaz: portance, masse ajoute et interactions hydrodynamiques.* PhD thesis, cole Centrale de Lyon, July 1992.

[7] P.G. Saffman. The lift on a small sphere in a slow shear flow. *Journal of Fluid Mechanics*, 22(02):385–400, 1965.

[8] J.B. McLaughlin. Inertial migration of a small sphere in linear shear flows. *J. Fluid Mech*, 224:261–274, 1991.

[9] J.B. McLaughlin. The lift on a small sphere in wall-bounded linear shear flows. *Journal of Fluid Mechanics*, 246:249–249, 1993.

[10] P. Cherukat and J.B. McLaughlin. The inertial lift on a rigid sphere in a linear shear flow field near a flat wall. *Journal of Fluid Mechanics*, 263:1–18, 1994.

[11] Evgeny S Asmolov et al. The inertial lift on a spherical particle in a plane poiseuille flow at large channel reynolds number. *Journal of Fluid Mechanics*, 381:63–87, 1999.

[12] P. Vasseur and RG Cox. The lateral migration of spherical particles sedimenting in a stagnant bounded fluid. *J. Fluid Mech*, 80(part 3):561–591, 1977.

[13] AM Ardekani, RH Rangel, and DD Joseph. Motion of a sphere normal to a wall in a second-order fluid. *Journal of Fluid Mechanics*, 587(1):163–172, 2007.

[14] I Eames. The concept of drift and its application to multiphase and multibody problems. *Philosophical Transactions of the Royal Society of London. Series A: Mathematical, Physical and Engineering Sciences*, 361(1813):2951–2965, 2003.

[15] Charles Darwin. Note on hydrodynamics. In *Proc. Camb. Phil. Soc*, volume 49, pages 342–354. Cambridge Univ Press, 1953.

[16] MJ Lighthill. Drift. *Journal of Fluid Mechanics*, 1(01):31–53, 1956.

[17] TR Auton, JCR Hunt, and M. Prud'Homme. The force exerted on a body in inviscid unsteady non-uniform rotational flow. *Journal of Fluid Mechanics*, 197(1):241–257, 1988.

[18] D. Legendre and J. Magnaudet. The lift force on a spherical bubble in a viscous linear shear flow. *Journal of Fluid Mechanics*, 368:81–126, 1998.

[19] M. Rastello, J.L. Marié, and M. Lance. Drag and lift forces on clean spherical and ellipsoidal bubbles in a solid-body rotating flow. *Journal of Fluid Mechanics*, 682(1):434–459, 2011.

[20] M. Rastello, J.L. Marié, N. Grosjean, and M. Lance. Drag and lift forces on interface-contaminated bubbles spinning in a rotating flow. *Journal of Fluid Mechanics*, 624(1):159–178, 2009.

[21] A. Tomiyama, H. Tamai, I. Zun, and S. Hosokawa. Transverse migration of single bubbles in simple shear flows. *Chemical Engineering Science*, 57(11):1849–1858, 2002.

[22] L. Zeng, S. Balachandar, and P. Fischer. Wall-induced forces on a rigid sphere at finite reynolds number. *Journal of Fluid Mechanics*, 536(1):1–25, 2005.

[23] J. Fang, J. Lu, A.M. Thomas, I.A. Bolotnov, and G. Tryggvason. Itm/dns database of drag, lift and wall effects, including the effects of void fractions. Technical report, CASL, 2013.

[24] R. Mei and JF Klausner. Shear lift force on spherical bubbles. *International journal of heat and fluid flow*, 15(1):62–65, 1994.

[25] W. Dijkhuizen, M. van Sint Annaland, and JAM Kuipers. Numerical and experimental investigation of the lift force on single bubbles. *Chemical Engineering Science*, 65(3):1274–1287, 2010.

[26] Hyungoo Lee and S Balachandar. Drag and lift forces on a spherical particle moving on a wall in a shear flow at finite re. *Journal of Fluid Mechanics*, 657:89–125, 2010.

[27] Ernst A Van Nierop, Stefan Luther, Johanna J Bluemink, Jacques Magnaudet, Andrea Prosperetti, and Detlef Lohse. Drag and lift forces on bubbles in a rotating flow. *Journal of Fluid Mechanics*, 571(1):439–454, 2007.

[28] F. Takemura, J. Magnaudet, and P. Dimitrakopoulos. Migration and deformation of bubbles rising in a wall-bounded shear flow at finite reynolds number. *Journal of Fluid Mechanics*, 634:463, 2009.

[29] Horace Lamb. *Hydrodynamics*. Cambridge university press, 1993.

[30] SP Antal, RT Lahey, and JE Flaherty. Analysis of phase distribution in fully developed laminar bubbly two-phase flow. *International Journal of Multiphase Flow*, 17(5):635–652, 1991.

[31] T. Frank, J. Shi, and A.D. Burns. Validation of eulerian multiphase flow models for nuclear safety application. In *Proceeding of the Third International Symposium on Two-Phase Modelling and Experimentation, Pisa, Italy*, 2004.

[32] SK Wang, SJ Lee, OC Jones, and RT Lahey. 3-d turbulence structure and phase distribution measurements in bubbly two-phase flows. *International Journal of multiphase flow*, 13(3):327–343, 1987.